Remote Sensing Applications: Society and Environment 34 (2024) 101161

Contents lists available at ScienceDirect

Remote Sensing Applications: Society and Environment

journal homepage: www.elsevier.com/locate/rsase

Temperate forest soil pH accurately Quantified with image spectroscopy

Haidi Abdullah [a, *], Andrew K. Skidmore [a], Andjin Siegenthaler [a], Devara P. Adiningrat [a], Yiwei Duan [a], Mélody Rousseau [a]

[a] *Faculty of Geo-Information Science and Earth Observation (ITC), University of Twente, PO Box 217, Drienerlolaan 5, 7500 AE Enschede, The Netherlands*

ARTICLE INFO

Keywords:
Soil acidification
Hyperspectral satellite
DESIS
Leaf and soil micronutrient concentrations
PLSR

ABSTRACT

Forest canopies to some extent obscure passive reflectance of soil traits such as pH, as well as below-canopy vegetation, in the optical to middle infrared portions of the electromagnetic spectrum (approximately 400–2500 nm) which are typically used in airborne and spaceborne image spectrometers. In this study, we present, for the first time, an accurate estimation of soil pH across extensive areas using hyperspectral imaging data obtained from the DLR Earth Sensing Imaging Spectrometer (DESIS) satellite. Furthermore, we investigate the impact of predicted soil pH variation on the concentrations of micronutrients in both leaves and soil. Our modelling is based on a comprehensive in-situ field campaign conducted during the summers of 2020 and 2021. This campaign collected soil pH data for model calibration and validation from 197 plots located across three distinct temperate forest sites: Veluwezoom and Hoge Veluwe National Parks in the Netherlands, as well as the Bavarian Forest National Park in Germany. The soil pH for each test site was accurately predicted by means of a partial least squares regression (PLSR) model, root mean square error ($RMSE_{cv}$) of 0.22 and the cross-validated coefficient of determination (R^2_{CV}) of 0.66. Our findings demonstrate that there are patches of extremely low soil pH possibly due to ongoing soil acidification processes. We saw a particularly significant decrease in soil pH ($p \leq 0.05$) in the coniferous forests when compared to the deciduous forest. The acidification of forest soils had a profound impact on the variation of soil and leaf micronutrient content, particularly iron concentration. These results highlight the potential of image spectroscopy data from the DESIS satellite to monitor and estimate soil pH in forested areas over extensive areas given sufficient data. Our findings hold significant implications for soil pH monitoring programs, enabling forest managers to assess the impact of their management practices and gauge their effectiveness in maintaining soil and forest vitality.

1. Introduction

Soil pH is a crucial factor in determining the composition and health of soil. It serves as a vital indicator of soil quality and has a significant impact on various aspects of forest health and ecosystem functioning (O'Neill 2005) by influencing different biological and chemical processes occurring in the soil (Rengel 2011; Neina 2019). For instance, the availability of essential nutrients like nitrogen, phosphorus, and potassium, are reduced under higher acidity thereby impacting tree growth and vitality (de Jong et al., 2022).

* Corresponding author.
E-mail address: h.j.abdullah-1@utwente.nl (H. Abdullah).

https://doi.org/10.1016/j.rsase.2024.101161
Received 8 September 2023; Received in revised form 7 December 2023; Accepted 26 December 2023
Available online 11 February 2024

Distinct tree species have specific soil pH preferences that directly impact nutrient availability for healthy development (Londo et al., 2006; Roell et al., 2022). Soil pH also plays a crucial role in influencing the activity and diversity of soil bacteria and fungi, which are essential for organic matter decomposition and nutrient cycling (Black et al., 2003; Tedersoo et al., 2020). Acidic soils present a considerable challenge in agricultural and forest areas as they hinder nutrient availability, restrict vegetation growth, and cause nutrient deficiencies by lowering the soil pH.

A key cause of soil acidification in forested regions is often attributed to the deposition of nitrogenous and acidic compounds aerially deposited in a dry or wet state (Abrahamsen 1984, de Jong et al., 2022) or by acidification processes in the soil (Huang et al., 2022). The so-called "acid rain" phenomena emerged as a significant challenge in Europe and North America in the early 1970s, with the major contributor to this being the atmospheric deposition of industrial nitrogen emissions resulting from power plants, factories, and vehicles burning fossil fuels (Moomaw 2002; Lajtha and Jones 2013). Regulations implemented in the 2000s, such as smokestack scrubbers and vehicle catalytic converters mitigated the problem of soil acidification caused by atmospheric deposition from industrial and transport nitrogen emissions (Basu 2007).

Despite the reduction in acid deposition from industrial sources, other factors continue to contribute to soil acidification. Natural processes such as the decomposition of (acidic) organic matter, including leaves and plant debris from particularly coniferous tree needles and twigs, can release organic acids that lower soil pH (Adeleke et al., 2017; Krishna and Mohan 2017). In addition, forest areas located near agricultural farmlands can undergo further acidification, such as excessive use of nitrogen-based fertilizers, including ammonium-based fertilizers, which release acidic compounds during nitrification, leading to soil acidification (Barak et al., 1997; Falkengren-Grerup et al., 2006).

Acidic soil with particularly low pH poses the risk of toxicity, particularly the release of heavy metals such as aluminium, which can be detrimental to tree roots, impairing their growth and overall health (Vrba et al., 2014; Kopačková et al., 2015), by affecting the functioning of tree roots, nutrient uptake, and overall tree vigour (Finlay 1995). Monitoring and measuring soil pH in forested regions yields valuable insights into the overall well-being and vigour of the forest ecosystem, aids in the early identification of soil acidification, and facilitates the implementation of suitable measures to counteract the issue and prevent further deterioration. Furthermore, the implementation of a soil pH monitoring program is indispensable during forest restoration and rehabilitation endeavours, for example by selecting the most appropriate tree species based on their specific pH requirements (Liu et al., 2011). Lastly, by monitoring soil pH, forest managers can assess the impact of continuing airborne deposition (especially) of nitrogenous compounds on soil pH.

Traditionally, foresters and park managers have relied on field surveys to assess soil pH in forested areas, using various methods like handheld pH meters, pH test strips, and laboratory analysis for soil sampling. These surveys are time-consuming, expensive, and inefficient, especially over large areas, and where there is significant variation in soil pH across large regions; often these approaches fail to provide accurate measurements at a fine scale and especially to locate pH 'hotspots' which can remain unsampled between the (necessarily) widely spaced in situ field samples.

To address the shortcomings of the traditional approach in measuring soil pH, one potential solution is to leverage remote sensing data. Remote sensing offers the ability to assess and estimate soil pH across large areas within relatively short timeframes (Ben-Dor 2002). By utilising remotely sensed data, it becomes possible to monitor changes in soil pH over time. Currently, the application of remote sensing for soil pH monitoring has primarily concentrated on agricultural farmlands (Ghazali et al., 2020; Webb et al., 2021). This focus on fallow agricultural land is because the traditionally available optical data (e.g., broadband satellite sensors with limited spectral bands) are not obscured by canopy cover – forests with a dense canopy cover (partially) obscure the direct measurement of soil pH. The forest canopy biochemical properties can be a proxy for soil pH measurements, given the direct and indirect influence of soil pH on nutrient availability in the soil and plant nutrient uptake processes, (Toro-Manríquez et al., 2019). Utilising image spectroscopy potentially provides the necessary spatial resolution as well as spectral resolution (i.e., those parts of the electromagnetic spectrum sensitive to soil pH), to more accurately map soil pH. For example, the DLR Earth Sensing Imaging Spectrometer (DESIS) hyperspectral satellite, launched on April 1, 2022, and operated by the German Aerospace Centre (DLR) has been designed in part to assess soil biochemical and biophysical properties (Chabrillat et al., 2019). This imaging spectrometer directly characterizes and resolves forest canopies using hundreds of spectral bands in the range of 400–1000 nm with a high spatial resolution (30 m) and radiometric resolution of 12 bits per pixel, allowing for the absorption characteristics associated with soil minerals and water content to be examined (Krutz et al., 2019).

This research introduces an innovative approach that utilizes imaging spectroscopy data obtained from the DESIS satellite to estimate soil pH in temperate forests situated in two distinct geographical locations, namely Germany and the Netherlands. Additionally, this study explores the effects of predicted soil pH variations across different forest stands and the levels of in-situ measured micronutrients in both soil and leaves, such as iron, phosphorus, calcium, magnesium and potassium. Our hypothesis is that the distinctive absorption features observed in forest canopy biochemical properties like chlorophyll, nitrogen, water content, and micronutrients, as well as some signal reflectance from canopy gaps, can yield accurate and robust estimates of forest soil pH over extensive areas.

2. Materials and methods

2.1. Study area

The focus here is on three temperate forests situated in distinct geographical locations within Europe. Specifically, our study sites are located in the Netherlands (Veluwezoom and the Hoge Veluwe National Park) and Germany (Bavarian Forest National Park). The Veluwezoom and Hoge Veluwe National Park are two adjacent natural forest reserves located in the central part of the Netherlands (Fig. 1). The Veluwezoom spans an area of approximately 50 km^2 and is situated in the province of Gelderland, near the town of Rheden, between the longitude 2°02′48.84″ and latitude 06°00′43.92″E (Plakman et al., 2020; Mols et al., 2021). The Veluwezoom en-

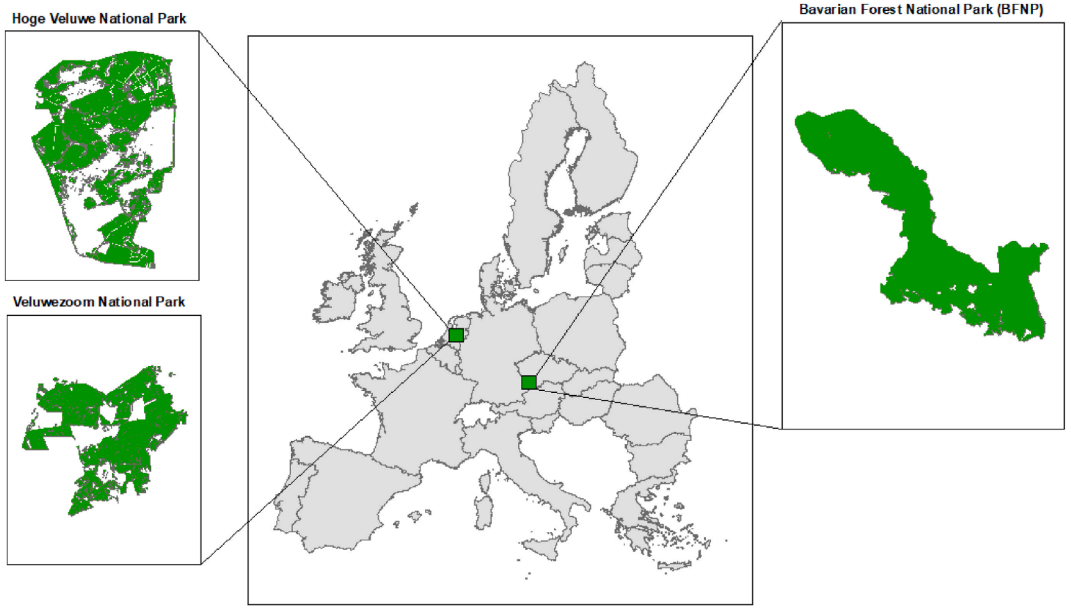

Fig. 1. The locations of the three study sites in the Bavarian Forest National Park, Germany, and Hoge Veluwe and Veluwezoom National Parks in the Netherlands.

compasses heathland and a mix of coniferous and deciduous forests, primarily composed of European beech, oak, birch, Scotch pine, and Norway spruce. The temperate climate of the area is characterized by an average annual temperature of 10.51 °C and precipitation of 850 mm.

The Hoge Veluwe National Park covers an area of approximately 55 km^2 and is situated in the eastern part of the Veluwezoom National Park, between the main cities of Arnhem, Ede, and Apeldoorn (Hein 2011). The Hoge Veluwe National Park boasts a diverse landscape consisting of sand dunes, heathlands, forests, and grasslands. The area shares similar climatic and tree species characteristics as the Veluwezoom.

The Bavarian Forest National Park is located in south-eastern Germany near the border with the Czech Republic and is part of the larger Bohemian Forest. The BFNP is situated at 13°12′9″ E and 49°3′19″ N and covers an area of approximately 240 km^2. The region has a temperate climate with abundant precipitation throughout the year, averaging around 1200–1800 mm annually. The BFNP is characterized by a mix of coniferous and deciduous forests. At higher elevations, Norway spruce dominates around 90% of the area, with the remaining 10% comprising of European beech and other deciduous trees (Abdullah et al., 2018a). In the hills and valley slopes, European beech covers approximately 83%, while Norway spruce makes up the rest of the forest. Full details regarding the BFNP can be found in (Lehnert et al., 2013). The BFNP, located in Germany, has experienced the detrimental effects of acid rain in the past, leading to a multitude of environmental issues within this national park (Beudert and Gietl 2015).

2.2. Data

2.2.1. Field data collection

Two field campaigns in 2020 and 2021 were conducted and a total of 197 soil plots were collected from three designated test sites: Bavarian Forest National Park, Hoge Veluwe and Veluwezoom (Fig. 1). The plots were distributed across coniferous and deciduous stands, with a criterion of >75% canopy dominance by a coniferous or deciduous forest type. In addition, sixteen plots consisted of mixed coniferous and deciduous stands with <75% canopy dominance. Each of the 197 selected plots measured 30 × 30 m to match the spatial resolution of DESIS data. This allowed for a 30-m radius buffer zone around the central pixel location to account for uncertainty in the spatial registration of image pixels (Abdullah et al., 2018a). The central point of each plot was determined using a Differential Global Positioning System (DGPS) Leica GPS 1200, which provided an accuracy of better than 1 m after post-processing.

Sampling occurred from June to August 2020 and May to August 2021, specifically when the broadleaved forest was fully mature and before senescence, thereby minimizing seasonal effects. In each plot, three composite topsoil samples (upper 10 cm) were collected from 3 × 3 m subplots in 2020, while two composite samples were collected in 2021. Each composite sample comprised a homogenized mixture of nine cores (10 cm height x 5 cm Ø, after removal of litter) collected in a 3 × 3 m grid. Large rocks and stones were removed from the samples, which were then oven-dried at 105 °C for 24 h and finely ground using a Retsch Planetary Ball Mill PM 200.

Top canopy leaf samples were collected from multiple tree branches within each plot using a large slingshot (Tree Runner BigShot) and a modified crossbow with rope (Abdullah et al., 2018b). A minimum of 40 leaves or 30 needle cohorts per tree were collected and directly oven-dried for 72 h at 65 °C, before being finely ground using a household blade coffee grinder.

Finally, soil pH-H2O was determined by dissolving 10 g of ground soil in ultra-pure water at a ratio of 1:2.5 (soil to water). The pH was then measured using a Metrohm 914 pH and conductivity meter, which has an accuracy of ±0.003 pH (Metrohm AG, Switzer-

land). The measurement followed the procedure outlined by Reeuwijk (2002). Similarly, soil micronutrients were determined using a handheld Thermo ScientificTM Niton Portable X-Ray Fluorescence analyzer, following the manufacturer's instructions. For leaf micronutrients, an Inductively Coupled Plasma - Optical Emission Spectrometry (PerkinElmer 8300DV ICP/OES) was utilized after open acid digestion of 200 mg of dried leaf material in a 6 ml mixture of 1:1 (vol:vol) hydrogen peroxide (analytical grade, 30%) and nitric acid (Suprapur, 65%).

2.2.2. Satellite data

The DLR Earth Sensing Imaging Spectrometer (DESIS) satellite data was utilized for the Bavarian Forest National Park test site in July 2020 and the Veluwezoom and Hoge Veluwe test sites in June 2020. The image data was collected synchronously with the field data collection. The DESIS satellite is a push-broom imaging spectrometer (hyperspectral imager) that provides hyperspectral images with 235 spectral bands over the visible and near-infrared regions of 400–1000 nm, with a spectral resolution of 2.55 nm and a spatial resolution of 30 m (Fig. 2). The radiometric resolution for each band is 12 bit with a 1 bit gain (Alonso et al., 2019).

In this study, the DESIS Level-2A product was used. The L2A product was delivered as standardized ortho-corrected as well as radiometrically-corrected reflectance. Furthermore, the L2A product provides the atmospherically corrected, terrain corrected, and includes several masks including water, cloud shadow, and haze that remove the effects of atmospheric interference from the sensor measurements, resulting in more accurate and reliable data (Krutz et al., 2019; Aneece et al., 2022).

2.3. Data pre-processing and partial least square regression

In order to prepare and standardize the DESIS L2A images for subsequent analysis, a number of pre-processing steps were taken. Initially, the spectral profile was evaluated to eliminate low-quality or noisy bands, specifically excluding wavelengths of 402.8 nm, 410.3 nm, and 999.5 nm from the analysis, leaving 232 spectra for analysis. The spectral reflectance values of sample plots were extracted from the DESIS scenes to facilitate.

To estimate soil pH using DESIS data we utilized a partial least squares regression (PLSR) which is a commonly and widely used technique to retrieve soil and vegetation properties using remote sensing data (Geladi and Kowalski 1986, Darvishzadeh et al., 2011; Jiang et al., 2016; Wang et al., 2020). The PLSR is a regression technique that is specifically developed to tackle the issue of multicollinearity, which is a common problem in hyperspectral data due to the high correlation among the input variables (spectral bands) (Geladi and Kowalski 1986, Carrascal et al., 2009). In other words, PLSR performs under circumstances where there is multicollinearity in the independent (explanatory) variables, which is commonly encountered in hyperspectral data (Wang et al., 2020). For more comprehensive information regarding PLSR, Geladi and Kowalski (1986) provide an excellent overview.

The PLSR technique establishes a linear relationship between a set of independent variables (X) and a group of dependent variables (Y) (Wold et al., 1993). In order to estimate soil pH using the PLSR model, we initially combined the collected reflectance and *in-situ* measurements from three different test sites (Veluwezoom, Hoge Veluwe, and Bavarian Forest National Park). This was done to create a universal model capable of working in various locations with similar conditions, such as tree species and land cover types. Consequently, we constructed the PLSR model using reflectance data from 197 plots as independent variables (X) and in-situ measurements of soil pH from 197 soil samples as the dependent variables (Y). To calibrate the model and determine the optimal number of components required for the PLSR model, we employed leave-one-out cross-validation. This cross-validation approach was utilized to prevent overfitting, whereby an additional component is added to the model only when the root mean square error of cross-validation (RMSEcv) decreases by at least 2% (Darvishzadeh et al., 2008). In this study, five components (factors) built the PLSR model (refer to Fig. S1 in the supplementary materials). Performance assessment of the PLSR model used the coefficient of determination (R2), root mean square error of predictions (RMSE), and the root mean square error of cross-validation (RMSEcv) by comparing

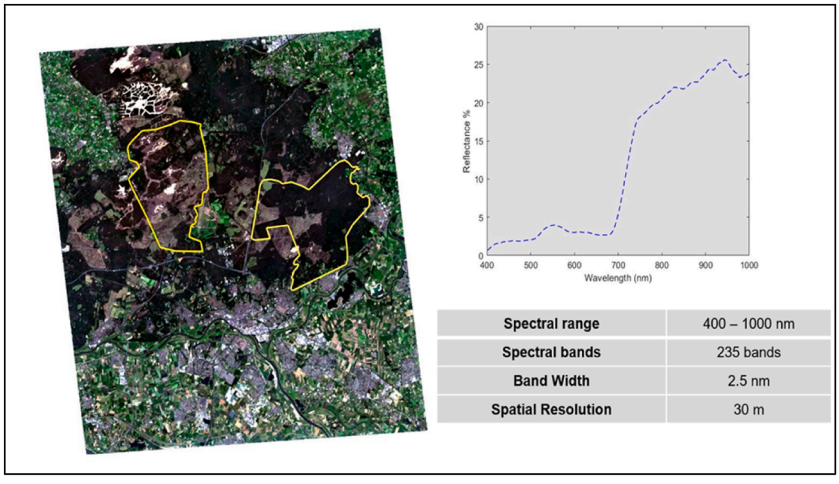

Spectral range	400 – 1000 nm
Spectral bands	235 bands
Band Width	2.5 nm
Spatial Resolution	30 m

Fig. 2. Shows the DESIS data acquired on June 23, 2020, over the Veluwezoom and Hoge Veluwe National Park in the Netherlands. The figure includes specifications of the DESIS data and an example of spectral reflectance data derived from DESIS data over a forested area in the Veluwezoom.

predicted and measured soil pH values. The significance of each spectral band estimated soil pH by calculating the variable 'importance in projection' (VIP). Furthermore, the impact of soil pH on each spectral band was calculated using the beta coefficient value. To determine the most informative spectral bands, our criteria involved selecting bands with VIP values greater than 1 while simultaneously considering the regression coefficient values, aiming for either the lowest or the highest values (Wold et al., 1993). MATLAB software (2019a) was used to conduct the PLSR analysis.

2.4. Model validation and mapping soil pH

To validate the performance of the PLSR model and generated soil pH maps, we employed a cross-validation technique known as leave-one-out (LOOCV). Given our sample size of 197 samples, we considered it inadequate for the conventional approach of splitting data into training and test sets (Berrar, 2018). Therefore, we have opted for Leave-One-Out Cross-Validation (LOOCV) to validate the performance of the Partial Least Squares Regression (PLSR) model. Moreover, our dataset comprises field data collected from three distinct locations. Randomly splitting the data into training and test sets could potentially result in a model that does not sufficiently represent the pH range across all three sites (Sammut and Webb, 2010). By choosing LOOCV, we ensure that each measured pH sample contributes to building the model, taking into account the unique characteristics of each site. This approach enhances the robustness of our model by considering the diversity in pH values across the different locations.

In LOOCV, each sample is temporarily excluded from the dataset, and the model is then trained on the remaining samples (Reunanen 2003). This process is repeated for all samples, amounting to 197 iterations. Subsequently, to evaluate the accuracy of the model, we computed the cross-validated root mean square error (RMSEcv) and cross-validated coefficient of determination (R_{cv}) based on the predicted and measured soil pH data. The model exhibiting the lowest RMSEcv value was chosen for generating the soil pH map (refer to Fig. S1 in the supplementary materials). Prior to the mapping procedure, we utilized land cover maps provided by the park administrations of Veluewzoom, Hoge Veluwe and Bavarian Forest National Park to identify forested land cover. For instance, in the case of Veluwezoom and Hoge Veluwe sites, we masked non-forested areas, such as sand dunes and heathlands. Similarly for BFNP, areas affected by bark beetle infestation such as dead wood and recently regenerating areas, were excluded as these areas were not sampled in our 197 field samples.

To cross-check the robustness of the generated soil pH maps, a comparison was made with existing soil pH data by utilising a soil pH map provided by the EUROPEAN SOIL DATA CENTRE (ESDAC) 2018, developed as part of the LUCAS project (Land Use and Land Cover Survey). The LUCAS project collected more than 22,000 soil samples from various member states of the European Union. Samples were largely from agricultural landscapes with few samples located in national park forests under limited or no human intervention. For more details on the LUCAS datasets and the methodology employed to generate the soil pH map, refer to Ballabio et al. (2019).

The soil pH map obtained from the LUCAS dataset was provided in a tiff file format, with a spatial resolution of 500 m per pixel. In order to facilitate the verification process and harmonize data, the LUCAS pH map was resampled to a resolution of 30 m, matching the spatial resolution of the DESIS data used in this study. Subsequently, to enable a comparison between the soil pH estimated in our study and the soil pH derived from the LUCAS dataset, 50 random samples were generated within each of the study sites Veluwezoom, Hoge Veluwe and Bavarian Forest National Park as depicted in Fig. 3. We extracted the corresponding soil pH values from both datasets for these samples. To evaluate the relationship between the two products, we computed the coefficient of determination, assessing their correlation.

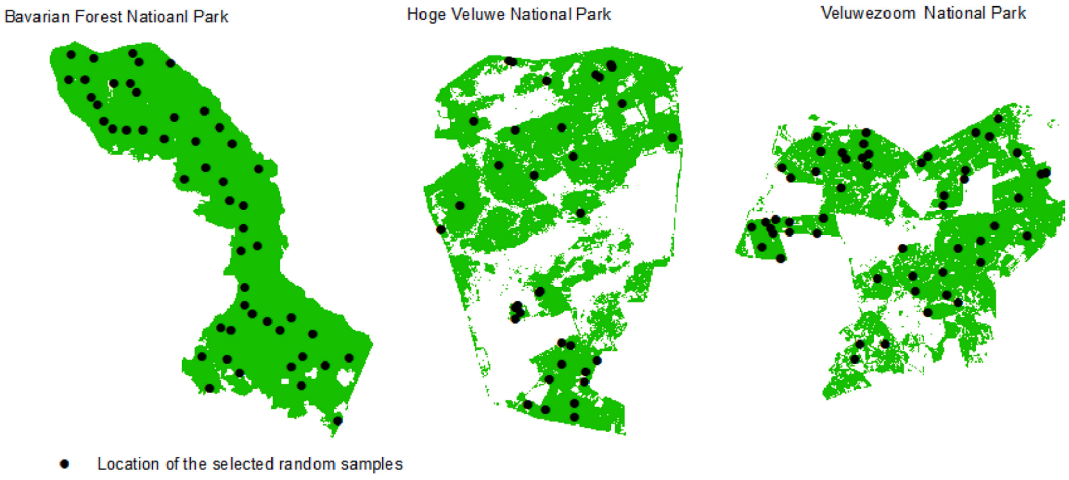

Fig. 3. Illustrates the placement and distribution of the randomly selected samples within the Veluwezoom, Hoge Veluwe, and Bavarian Forest National Park study areas.

3. Results

3.1. Soil pH mapping and validation

Fig. 4 illustrates the soil pH estimated by the PLSR model in comparison to the soil pH measured during the two field campaigns. The PLSR model has an R^2 value of 0.66 and an RMSEcv value of 0.22. We examined the contribution of each spectral band in the PLSR model for soil pH prediction by calculating the Variable importance in the projection (VIP) and regression coefficient (beta). Table 1 and Fig. 5 demonstrate a strong correlation between the spectral bands with VIP values exceeding 1 and the lowest or highest ± regression coefficients for the same bands. Generally, the most significant spectral bands for estimating soil pH are spread across the spectral range of DESIS data, ranging from 400 to 1000 nm. Nevertheless, the highest peaks predominantly occur in the red-edge region of 698–734 nm and the near-infrared region of 938–978 nm.

Utilising the PLSR model, we generated soil pH maps to visualize the spatial distribution across three prominent areas: the Bavarian Forest National Park, Veluwezoom, and Hoge Veluwe National Parks (Fig. 6a, b, and c). To conduct a more in-depth analysis of

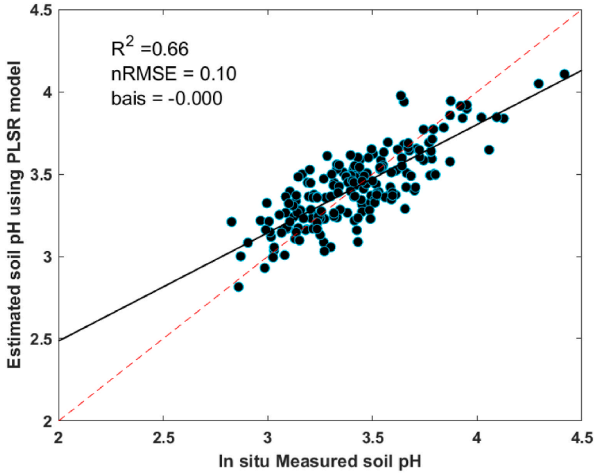

Fig. 4. Measured versus predicted soil pH derived from the PLSR analysis and DESIS Image spectroscopy data.

Table 1
Displays the spectral bands (nm) that were selected based on their Variable Importance in the Projection (VIP) scores and regression coefficient values.

	Visible	Red edge	Near Infrared
VIP	427, **437**, 517-**520**	**697–734**,**760**,767	**918**,**930–931**,942,**949**,**957**,**965**,981,988
Regression coefficient peak ±	**437**, **520**	**697–726**, **760**	**918**, **930–931**, **949**, **957**, **965**, 976

Note: In Table 1, the spectral bands highlighted in bold indicate the spectral bands that were selected using both the Variable Importance in the Projection (VIP) approach and the regression coefficient approach.

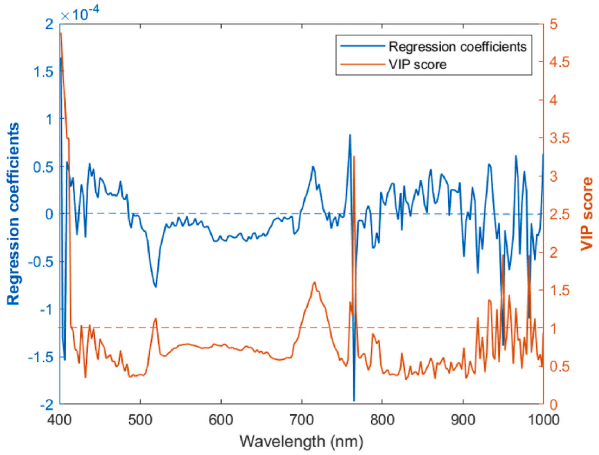

Fig. 5. The VIP scores and regression coefficients for soil pH generated by the PLSR analysis for the three ecosystems. VIP scores above the red dash line (VIP <1) indicate important band ranges for soil pH estimation. (For interpretation of the references to colour in this figure legend, the reader is referred to the Web version of this article.)

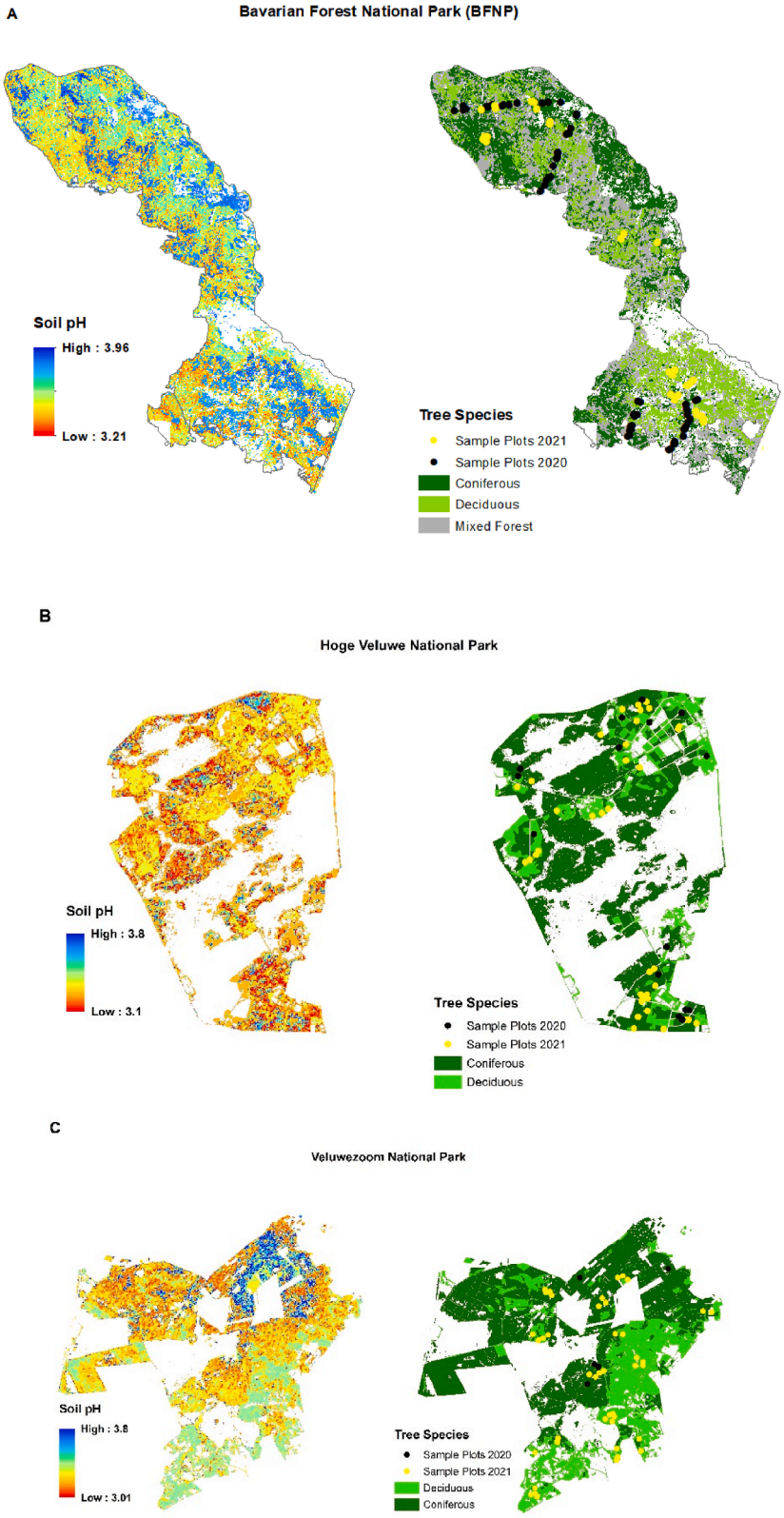

Fig. 6. Spatial distribution of estimated soil pH using DESIS data and the PLSR model over the Bavarian Forest National Park (a), Hoge Veluwe (b), and Veluwezoom National Park (c).

the soil pH maps, we employed the tree species maps developed by the park administrations. These tree species maps were utilized to extract the estimated soil pH value for each tree species, which was then compared to the in-situ measured soil pH data per tree species (Fig. 6). The results show a strong agreement between the modelled soil pH and the in-situ measured soil pH data, particularly for deciduous and coniferous trees in all three study sites (Fig. 7). However, it's important to note that a significantly ($P < 0.05$) lower soil pH was observed for the modelled soil pH in the Bavarian Forest National Park over the deciduous stands (Fig. 7).

Finally, to cross-check the robustness and verify the generated soil pH maps, a comparison was conducted with existing LUCAS soil pH data obtained from the European Soil Data Centre (ESDAC). A strong correlation is evident between the soil pH maps predicted by the PLSR model using our field data and the soil pH map generated with the LUCAS soil data (Fig. 8). The coefficient of determination (R^2) was 0.53 (Bavarian Forest National Park), 0.66 (Hoge Veluwe), and 0.69 (Veluwezoom), respectively, indicating a good match between the generated soil pH maps and the LUCAS pH map.

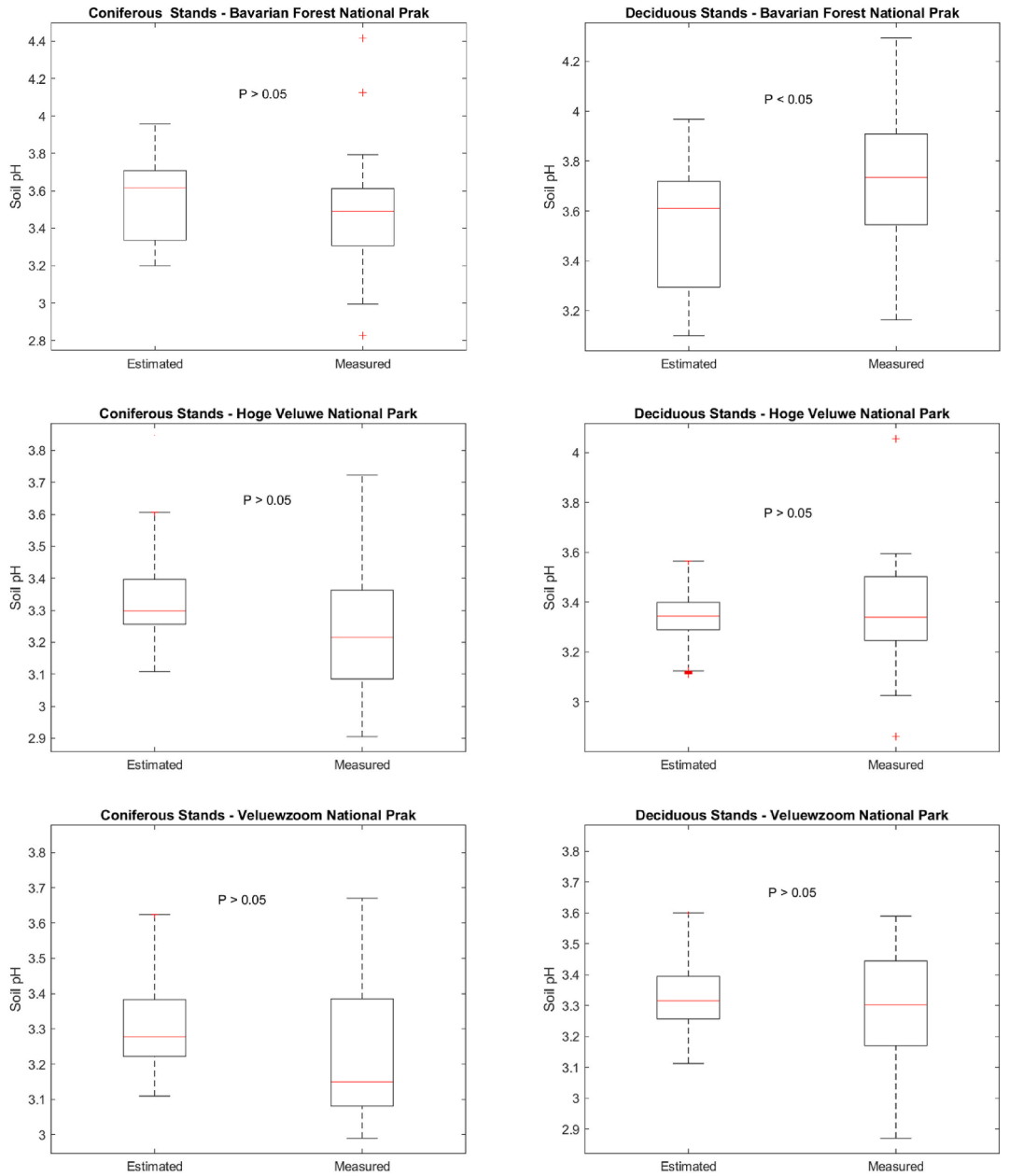

Fig. 7. Comparison of measured and estimated Soil pH in different tree species (Deciduous and Coniferous) across Bavarian Forest National Park, Hoge Veluwe, and Veluwezoom National Park.

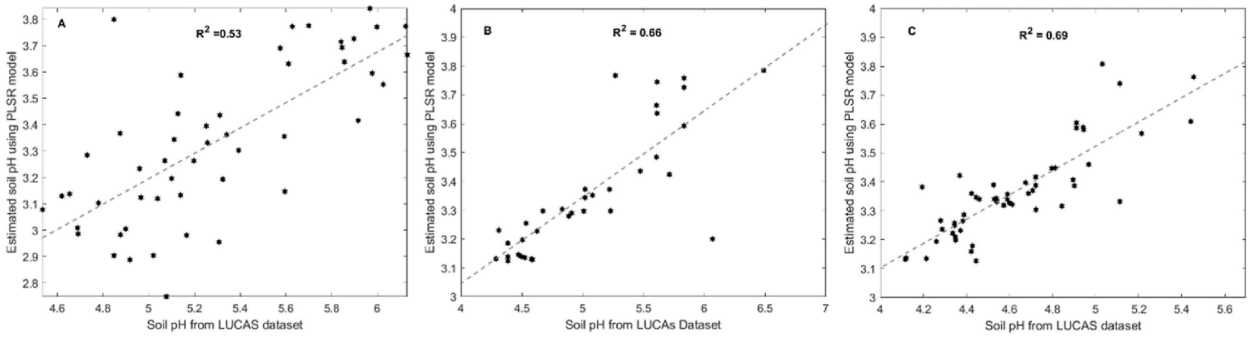

Fig. 8. Comparison of estimated soil pH using PLSR model and DESIS data against LUCASE soil pH data provided by EUROPEAN SOIL DATA CENTRE (ESDAC) across Bavarian Forest National Park (a), Hoge Veluwe (b), and Veluwezoom National Park (c).

3.2. The impact of soil pH on the variation of micronutrient concentrations in leaves and soil

The field-measured concentrations of micronutrients in leaves and soil from deciduous and coniferous stands are detailed in Tables 2 and 3. In the Bavarian Forest National Park, the average values of all the micronutrients (calcium, magnesium, potassium, phosphorus, and iron) were higher in deciduous stands compared to coniferous stands. This trend was similarly observed in the Hoge Veluwe and Veluwezoom national parks, with the exception of leaf Iron content, where both coniferous and deciduous stands exhibited values of 59 and 58 ppm, respectively.

To understand the influence of soil pH on the measured concentrations of micronutrients in both leaves and soil, we employed multiple linear regression, which revealed a significant ($p < 0.05$) and positive correlation between soil pH and leaf magnesium concentrations in both the Bavarian Forest National Park and the Hoge Veluwe and Veluwezoom National Parks. Similarly, soil pH demonstrates a notable positive impact ($p < 0.05$) on leaf and soil iron content. No substantial effects were observed for the other measured micronutrients (calcium, phosphorus, and potassium) in leaves and soil, except for the case of soil potassium concentration in the Hoge Veluwe and Veluwezoom National Parks. It is noteworthy that our results show that soil pH exhibits a positive influence on all measured soil and leaf micronutrient concentrations (refer to Figs. S2, S3, S4 and S5 in the supplementary materials).

4. Discussion

Our findings indicate that forest soil pH can be accurately estimated using image spectroscopy data from the DESIS satellite. Despite the challenges posed by the forest canopies of the study areas obstructing direct soil reflectance, we demonstrate it is possible to estimate soil pH from satellite image spectroscopy in forested areas with ($R^2 = 0.66$) accuracy. Previously, Šestak et al. (2019) and

Table 2
Displays the mean ± SD (standard deviation) of the measured leaf micronutrient concentrations (ppm) in coniferous and deciduous stands. The p-values indicate the influence of soil pH on leaf micronutrient content, with a (+) sign denoting a positive effect.

	Iron		Calcium		Phosphorus		Potassium		Magnesium	
BFNP	Mean	SD	Mean	SD	Mean	SD	Mean	SD	Mean	SD
Deciduous	71	14	4564	1576	1537	507	8716	1475	1274	374
Coniferous	55	15	3424	1519	1302	248	5803	1375	930	352
P- value	(+) < 0.001		0.67		0.169		0.20		(+) < 0.001	
NL										
Deciduous	58	12	2953	912	2149	1170	10,379	5143	1779	731
Coniferous	59	16	2814	1027	1115	241	4983	1145	862	403
P- value	(+) < 0.001		0.07		0.32		0.2		(+) < 0.001	

Table 3
Displays the mean ± SD (standard deviation) of the measured soil micronutrient concentrations (ppm) in coniferous and deciduous stands. The p-values indicate the influence of soil pH on soil micronutrient content, with a (+) sign denoting a positive effect.

	Iron		Phosphorus		Potassium	
BFNP	Mean	SD	Mean	SD	Mean	SD
Deciduous	16,190	2503	3619	3181	2531	2378
Coniferous	11,012	4502	3213	2826	2666	2421
P- value	(+) < .001		.261		.105	
NL						
Deciduous	2113	1222	602	92	2488	779
Coniferous	1774	1157	580	130	1669	638
P- value	(+) .027		0.75		(+) .0025	

Zhang et al. (2018) employed field spectrometers to gather soil spectra, resulting in moderate to good accuracy (with R^2 ranging from 0.5 to 0.69) in their soil pH estimations; it should be emphasized that these results are not directly comparable to ours since they focused on the field-scale level, used field (point-based) spectrometers and did not predict soil pH with an imaging spectrometer as used here.

Our findings show that the forest sites under investigation were in general extremely acidic with pH values below 4 as illustrated in Figs. 6 and 7. Some areas of the Dutch forests (Hoge Veluwe and Veluwezoom) had field-measured soil pH as low as 3.1, and our map predictions using DESIS idenitifed several new hotspots of extremely low soil pH (Fig. 6). One of the main causes of soil acidification in the Netherlands is the intensive practice of agriculture and livestock husbandry in the central, eastern, and southern parts of the country. This has led to an increase in atmospheric deposition of nitrogenous compounds, resulting in soil acidification (van Straalen et al., 1988; Bobbink 2021). On the other hand, our Bavarian Forest National Park site, affected by industrial (sulphorous and nitrogenous compound) acid rain particularly in the 1970s–1990s, caused extensive soil acidification (Zechl et al., 1990). Industrial emission controls since the 1980s has resulted in the partial recovery of organic layers and mineral topsoil, though deeper soil layers in acid-sensitive substrates continue to face further acidification (Meesenburg et al., 2019; Vrba et al., 2014).

Another important finding emerged from our results, namely a significant disparity in soil pH between coniferous and deciduous stands across all three forest locations. Notably, the observed soil pH range within the coniferous stands was consistently lower and more acidic compared to the deciduous stands. This finding adds further weight to the importance of understanding the contrasting soil conditions in these 2 distinct forest types (Fig. 7). Coniferous litter is generally more acidic than deciduous litter due to the accumulation of acidic organic matter from needles and the release of organic acids by coniferous root systems. Consequently, the soil under coniferous stands generally has a lower pH (Chodak et al., 2016; Klimek et al., 2020), as confirmed in Fig. 7c for the northern part of Veluwezoom National Park as well as for BFNP (Fig. 6a). Which is predominantly occupied by coniferous stands.

The relationship between soil pH and vegetation canopy reflectance is rooted in the influence of soil chemical properties on the health and physiological processes of plants. For example, in this study some of the spectral bands in DESIS imagery found to be important for estimating soil pH (Fig. 5 and Table 1) included band 437 nm which is known to be influenced by the biochemical properties of plants, particularly chlorophyll content (Gitelson et al., 1999). The red edge (697–734 nm) is also associated with chlorophyll absorption in plants, in addition to being a change indicator for plant stress and leaf nitrogen content (Abdullah et al., 2018b). Recent studies have investigated the impact of acidic rain on leaf chlorophyll content, revealing that acidic soil can reduce leaf chlorophyll content by an average of 6.7% per pH unit (Du et al., 2017). This finding highlights the potential of chlorophyll content as a proxy for estimating soil pH. Moreover, investigations have demonstrated that the spectral band at 519 nm is sensitive to leaf pigments, particularly chlorophyll content and photosynthetic activity (Gitelson et al., 2003; Hogewoning et al., 2012), as well as corresponding to the absorption of soil Fe content (Ben-Dor et al., 2008). Given the connection between leaf and soil Fe content (Irmak et al., 2008), this spectral band can offer insights into variations in Fe content between soil and leaves.

The enhanced resolution of DESIS imagery, when contrasted with previous satellites like MERIS, holds the potential to identify finer details such as smaller canopy gaps within forests. This heightened capability could facilitate the detection of canopy gaps linked to lower pH levels in the forest ecosystem. By capturing these intricate features, the higher resolution of next-generation satellite image spectroscopy such as DESIS could provide valuable insights into the ecological health of forests and their response to changing environmental conditions.

Typically, a negative correlation exists between iron availability and soil pH, as acidic soil enhances the solubility of iron compounds, affecting their availability and mobility (refer to Fig. S6 in the supplementary materials). Consequently, Fe compounds dissolve more readily in acidic soil (pH 4–5), releasing Fe ions into the soil solution and making them more accessible for plant uptake (Hartemink and Barrow 2023). However, our micronutrient measurements of soil and leaf samples yielded unexpected results. As depicted in Tables 1 and 2, the iron content was lower in both leaf and soil samples from coniferous stands compared to deciduous stands. Despite acidic soil conditions potentially impacting iron availability and uptake by plants, changes occur in highly acidic soils ($pH < 4$) that reduce the iron's accessibility for plant uptake (Bastianelli, Ali et al. 2017). These changes involve the formation of insoluble iron compounds that are less accessible to plants (Truog 1947). Thus, these alterations may explain the findings of our study, as the soil pH at all study sites was extremely low, below 4.

Furthermore, it is noteworthy that the absorption region around 520 nm was responsive to the calcium, phosphorus, and magnesium content in the leaves. When these micronutrients become depleted, the reflectance at 520 nm tends to increase (Ayala-Silva and Beyl 2005). This phenomenon can be attributed to the critical role that calcium, magnesium, and phosphorus play in the growth and development of plants (Malhotra et al., 2018). Insufficient levels of any of these micro- and macro-nutrients in plants can lead to physiological and morphological alterations. For example, magnesium is essential for chlorophyll formation (Cakmak and Yazici 2010), while phosphorus is necessary for energy transmission and storage (Duff et al., 1994). Calcium, on the other hand, is vital for constructing cell walls and facilitating membrane function (Demarty et al., 1984). Essentially, a decline in calcium, magnesium, and phosphorus levels can result in reduced chlorophyll content and overall plant biomass, consequently causing an increase in reflectance at 520 nm (Weng et al., 2022). Similarly, when plants experience a decrease in calcium, magnesium, and phosphorus levels, the reflectance in the near-infrared (NIR) region, 950–980 nm typically decreases (Belgiu et al., 2023). The reduction in reflectance can be attributed to a decline in leaf water content, as supported by previous studies (Slaton et al., 2001, Abdullah, Skidmore et al. 2019). This decrease in leaf water content often occurs when plant nutrients are scarce. In simpler terms, when the plant's nutritional levels are low, it may allocate less water to the leaves, resulting in reduced leaf water content. The findings from the analysis of leaf micronutrient concentrations (Tables 2 and 3) further substantiate this point, as they indicate lower levels of calcium, magnesium, and phosphorus within the coniferous stands compared to the deciduous stands.

The results showed a strong agreement between the estimated soil pH in our study and the soil pH data from the LUCAS dataset (Ballabio et al., 2019). This finding indicates the reliability and accuracy of our pH estimation approach, bolstering the confidence in the results obtained for the study areas (Fig. 8). However, it is crucial to recognize that the LUCAS dataset lacks soil samples specifically collected from our three test sites (Hoge Veluwe, Veluwezoom, and Bavarian Forest National Park). Consequently, relying solely on the LUCAS dataset for soil pH measurements, and not specifically sampling in these specific study sites may lead to potential inaccuracies due to under-sampling of in-situ soil measurements in the LUCAS dataset not adequately representing the soil conditions for our study sites. Therefore, our study's independent estimation of soil pH serves as a valuable contribution ensuring a more robust and site-specific assessment of soil conditions in these ecologically important areas.

5. Conclusion

The findings of this study demonstrate the potential of hyperspectral data derived from image spectroscopy satellites such as DESIS for accurate estimation of soil pH under forest canopies which obstruct direct remote sensing of the ground. We identified specific spectral bands within the visible spectrum, namely 419 and 519 nm, as well as ranges between 697-734 nm and 918–965 nm in the red-edge and NIR regions, which displayed the highest VIP and regression coefficient values. These bands proved to be crucial in estimating soil pH. Additionally, we investigated the correlation between leaf and soil micronutrient concentrations, including iron, phosphorus, magnesium, potassium, and calcium, and the identified spectral bands for estimating soil pH. In conclusion, we present novel evidence that the DESIS image spectroscopy data holds great promise for estimating soil pH within forested areas. Moreover, the examination of the relationship between leaf traits, soil pH, and hyperspectral data represents a crucial step towards enhancing our comprehension of the link between Earth observation data and forest canopy cover as a proxy for estimating soil pH. It is important to note that the image spectroscopy data obtained from the DESIS satellite covers a spectral range of 400–1000 nm. Therefore, further research focusing on different image spectroscopy from the enhanced spectral range (400–2500 nm) available from the PRISMA and EnMap satellites, may further enhance the utilization of remote sensing data in estimating soil pH in forested areas.

Funding

This research was funded by European Research Council (ERC) under the European Union's Horizon 2020 research and innovation programme (grant agreement n° 834709).

Ethical statement

We admit that to the best of the authors' knowledge, this submission has no potential ethical issues.

CRediT authorship contribution statement

Haidi Abdullah: Conceptualization, Formal analysis, Methodology, Software, Validation, Visualization, Writing – original draft, Writing – review & editing. **Andrew K. Skidmore:** Conceptualization, Funding acquisition, Supervision, Writing – original draft, Writing – review & editing. **Andjin Siegenthaler:** Writing – original draft, Writing – review & editing. **Devara P. Adiningrat:** Writing – review & editing. **Yiwei Duan:** Writing – review & editing. **Mélody Rousseau:** Writing – review & editing.

Declaration of competing interest

The authors declare that they have no known competing financial interests or personal relationships that could have appeared to influence the work reported in this paper.

Data availability

The authors do not have permission to share data.

Acknowledgements

The research was funded through the BIOSPACE project, which received financial support from the European Research Council (ERC) within the framework of the European Union's Horizon 2020 research and innovation programme, as indicated by grant agreement number 834709. The authors would like to express their sincere appreciation for the support received during the field data collection process from the Bavarian Forest National Park (BNFP), as well as from the contributors to the "Data Pool Forestry" initiative, the Bavarian State Forest Enterprise (Bayerische Staatsforsten), and Neuburg Forest in Germany. We are also grateful for the support provided by the Hoge Veluwe National Park, Veluwezoom National Park, and Royal Estate Het Loo in the Netherlands. The authors express gratitude to the members of the BIOSPACE project, in particular A. Torres Rodriguez, Dr. E. Neinavaz, R. Darvishzadeh, and T. Wang, for their assistance during the fieldwork campaign and data collection.

Appendix A. Supplementary data

Supplementary data to this article can be found online at https://doi.org/10.1016/j.rsase.2024.101161.

References

Abdullah, H., Darvishzadeh, R., Skidmore, A.K., Groen, T.A., Heurich, M., 2018a. European spruce bark beetle (Ips typographus, L.) green attack affects foliar reflectance and biochemical properties. Int. J. Appl. Earth Obs. Geoinf. 64, 199–209.

Abdullah, H., Skidmore, A.K., Darvishzadeh, R., Heurich, M., 2019. Timing of red-edge and shortwave infrared reflectance critical for early stress detection induced by bark beetle (Ips typographus, L.) attack. Int. J. Appl. Earth Obs. Geoinf. 82.

Abdullah, H., Skidmore, A.K., Darvishzadeh, R., Heurich, M., Pettorelli, N., Disney, M., 2018b. Sentinel-2 accurately maps green-attack stage of European spruce bark beetle (Ips typographus, L.) compared with Landsat-8. Remote Sensing in Ecology and Conservation 5 (1), 87–106.

Abrahamsen, G., 1984. Effects of acidic desposition on forest soil and vegetation. Philos. Trans. R. Soc. Lond. B Biol. Sci. 305 (1124), 369–382.

Adeleke, R., Nwangburuka, C., Oboirien, B., 2017. Origins, roles and fate of organic acids in soils: a review. South Afr. J. Bot. 108, 393–406.

Alonso, K., Bachmann, M., Burch, K., Carmona, E., Cerra, D., de Los Reyes, R., Dietrich, D., Heiden, U., Holderlin, A., Ickes, J., Knodt, U., Krutz, D., Lester, H., Muller, R., Pagnutti, M., Reinartz, P., Richter, R., Ryan, R., Sebastian, I., Tegler, M., 2019. Data products, quality and validation of the DLR Earth sensing imaging spectrometer (DESIS). Sensors 19 (20).

Aneece, I., Foley, D., Thenkabail, P., Oliphant, A., Teluguntla, P., 2022. New generation hyperspectral data from DESIS compared to high spatial resolution PlanetScope data for crop type Classification. IEEE J. Sel. Top. Appl. Earth Obs. Rem. Sens. 15, 7846–7858.

Ayala-Silva, T., Beyl, C.A., 2005. Changes in spectral reflectance of wheat leaves in response to specific macronutrient deficiency. Adv. Space Res. 35 (2), 305–317.

Ballabio, C., Lugato, E., Fernández-Ugalde, O., Orgiazzi, A., Jones, A., Borrelli, P., Montanarella, L., Panagos, P., 2019. Mapping LUCAS topsoil chemical properties at European scale using Gaussian process regression. Geoderma 355, 113912.

Barak, P., Jobe, B.O., Krueger, A.R., Peterson, L.A., Laird, D.A., 1997. Effects of long-term soil acidification due to nitrogen fertilizer inputs in Wisconsin. Plant Soil 197 (1), 61–69.

Bastianelli, C., Ali, A.A., Beguin, J., Bergeron, Y., Grondin, P., Hély, C., Paré, D., 2017. Boreal coniferous forest density leads to significant variations in soil physical and geochemical properties. Biogeosciences 14 (14), 3445–3459.

Basu, S., 2007. Chemical and biochemical processes for NOx control from combustion off-gases. Chem. Eng. Commun. 194 (10), 1374–1395.

Belgiu, M., Marshall, M., Boschetti, M., Pepe, M., Stein, A., Nelson, A., 2023. PRISMA and Sentinel-2 Spectral Response to the Nutrient Composition of Grains, vol. 292. Remote Sensing of Environment.

Ben-Dor, E., 2002. Quantitative Remote Sensing of Soil Properties.

Ben-Dor, E., Taylor, R.G., Hill, J., Demattê, J.A.M., Whiting, M.L., Chabrillat, S., Sommer, S., 2008. Imaging Spectrometry for soil applications. Adv. Agron. ume 97, 321–392.

Beudert, B., Gietl, G., 2015. Long-term monitoring in the Große Ohe catchment, bavarian forest national Park. Silva Gabreta 21 (1), 5–27.

Black, H.I.J., Parekh, N.R., Chaplow, J.S., Monson, F., Watkins, J., Creamer, R., Potter, E.D., Poskitt, J.M., Rowland, P., Ainsworth, G., Hornung, M., 2003. Assessing soil biodiversity across Great Britain: national trends in the occurrence of heterotrophic bacteria and invertebrates in soil. J. Environ. Manag. 67 (3), 255–266.

Bobbink, R., 2021. Effecten van stikstofdepositie nu en in 2030: een analyse. In: Onderzoekcentrum B-WARE. Nijmegen. Rapportnummer RP-20.135 **21**.

Cakmak, I., Yazici, A.M., 2010. Magnesium: a forgotten element in crop production. Better crops 94 (2), 23–25.

Carrascal, L.M., Galván, I., Gordo, O., 2009. Partial least squares regression as an alternative to current regression methods used in ecology. Oikos 118 (5), 681–690.

Chabrillat, S., Ben-Dor, E., Cierniewski, J., Gomez, C., Schmid, T., van Wesemael, B., 2019. Imaging spectroscopy for soil mapping and monitoring. Surv. Geophys. 40, 361–399.

Chodak, M., Klimek, B., Niklińska, M., 2016. Composition and activity of soil microbial communities in different types of temperate forests. Biol. Fertil. Soils 52 (8), 1093–1104.

Darvishzadeh, R., Atzberger, C., Skidmore, A., Schlerf, M., 2011. Mapping grassland leaf area index with airborne hyperspectral imagery: a comparison study of statistical approaches and inversion of radiative transfer models. ISPRS J. Photogrammetry Remote Sens. 66 (6), 894–906.

Darvishzadeh, R., Skidmore, A., Schlerf, M., Atzberger, C., 2008. Inversion of a radiative transfer model for estimating vegetation LAI and chlorophyll in a heterogeneous grassland. Rem. Sens. Environ. 112 (5), 2592–2604.

de Jong, A., de Vries, W., Kros, H., Spijker, J., 2022. Impacts of harvesting methods on nutrient removal in Dutch forests exposed to high-nitrogen deposition. Ann. For. Sci. 79 (1).

Demarty, M., Morvan, C., Thellier, M., 1984. Calcium and the cell wall. Plant Cell Environ. 7 (6), 441–448.

Du, E., Dong, D., Zeng, X., Sun, Z., Jiang, X., de Vries, W., 2017. Direct effect of acid rain on leaf chlorophyll content of terrestrial plants in China. Sci. Total Environ. 605–606, 764–769.

Duff, S.M., Sarath, G., Plaxton, W.C., 1994. The role of acid phosphatases in plant phosphorus metabolism. Physiol. Plantarum 90 (4), 791–800.

Falkengren-Grerup, U., Brink, D.-J. t., Brunet, J., 2006. Land use effects on soil N, P, C and pH persist over 40–80 years of forest growth on agricultural soils. For. Ecol. Manag. 225 (1), 74–81.

Finlay, R., 1995. Interactions between soil acidification, plant growth and nutrient uptake in ectomycorrhizal associations of forest trees. Ecol. Bull. 197–214.

Geladi, P., Kowalski, B.R., 1986. Partial least-squares regression: a tutorial. Anal. Chim. Acta 185, 1–17.

Ghazali, M.F., Wikantika, K., Harto, A.B., Kondoh, A., 2020. Generating soil salinity, soil moisture, soil pH from satellite imagery and its analysis. Information Processing in Agriculture 7 (2), 294–306.

Gitelson, A.A., Buschmann, C., Lichtenthaler, H.K., 1999. The chlorophyll fluorescence ratio F735/F700 as an accurate measure of the chlorophyll content in plants. Rem. Sens. Environ. 69 (3), 296–302.

Gitelson, A.A., Gritz, Y., Merzlyak, M.N., 2003. Relationships between leaf chlorophyll content and spectral reflectance and algorithms for non-destructive chlorophyll assessment in higher plant leaves. J. Plant Physiol. 160 (3), 271–282.

Hartemink, A.E., Barrow, N.J., 2023. Soil pH - nutrient relationships: the diagram. Plant Soil 486 (1–2), 209–215.

Hein, L., 2011. Economic benefits generated by protected areas: the case of the Hoge Veluwe forest, The Netherlands. Ecol. Soc. 16 (2).

Hogewoning, S.W., Wientjes, E., Douwstra, P., Trouwborst, G., van Ieperen, W., Croce, R., Harbinson, J., 2012. Photosynthetic Quantum yield Dynamics: from Photosystems to leaves. Plant Cell 24 (5), 1921–1935.

Huang, X., Cui, C., Hou, E., Li, F., Liu, W., Jiang, L., Luo, Y., Xu, X., 2022. Acidification of soil due to forestation at the global scale. For. Ecol. Manag. 505, 119951.

Irmak, S., Surucu, A., Aydin, S., 2008. The effects of iron content of soils on the iron content of plants in the Cukurova region of Turkey. Int. J. Soil Sci. 3 (3), 109–118.

Jiang, Q., Chen, Y., Guo, L., Fei, T., Qi, K., 2016. Estimating soil organic carbon of cropland soil at different levels of soil moisture using VIS-NIR spectroscopy. Rem. Sens. 8 (9), 755.

Klimek, B., Chodak, M., Niklińska, M., 2020. Soil respiration in seven types of temperate forests exhibits similar temperature sensitivity. J. Soils Sediments 21 (1), 338–345.

Kopačková, V., Lhotáková, Z., Oulehle, F., Albrechtová, J., 2015. Assessing forest health via linking the geochemical properties of a soil profile with the biochemical parameters of vegetation. Int. J. Environ. Sci. Technol. 12 (6), 1987–2002.

Krishna, M.P., Mohan, M., 2017. Litter decomposition in forest ecosystems: a review. Energy, Ecology and Environment 2 (4), 236–249.

Krutz, D., Muller, R., Knodt, U., Gunther, B., Walter, I., Sebastian, I., Sauberlich, T., Reulke, R., Carmona, E., Eckardt, A., Venus, H., Fischer, C., Zender, B., Arloth, S., Lieder, M., Neidhardt, M., Grote, U., Schrandt, F., Gelmi, S., Wojtkowiak, A., 2019. The Instrument Design of the DLR Earth sensing imaging spectrometer (DESIS). Sensors 19 (7).

Lajtha, K., Jones, J., 2013. Trends in cation, nitrogen, sulfate and hydrogen ion concentrations in precipitation in the United States and Europe from 1978 to 2010: a new look at an old problem. Biogeochemistry 116, 303–334.

Lehnert, L.W., Bässler, C., Brandl, R., Burton, P.J., Müller, J., 2013. Conservation value of forests attacked by bark beetles: highest number of indicator species is found in early successional stages. J. Nat. Conserv. 21 (2), 97–104.

Liu, X., Lu, Y., Zhou, Y., Lei, X., Zhang, X., Meng, J., 2011. The influence of soil conditions on regeneration establishment for degraded secondary forest restoration, Southern China. For. Ecol. Manag. 261 (11), 1771–1780.

Londo, A.J., Kushla, J.D., Carter, R.C., 2006. Soil pH and tree species suitability in the south. Southern Regional Extension Forestry 2, 1–5.
Malhotra, H., Vandana, S. Sharma, Pandey, R., 2018. Phosphorus nutrition: plant growth in response to deficiency and excess. Plant nutrients and abiotic stress tolerance 171–190.
Meesenburg, H., Riek, W., Ahrends, B., Eickenscheidt, N., Grüneberg, E., Evers, J., Fortmann, H., König, N., Lauer, A., Meiwes, K.J., Nagel, H.-D., Schimming, C.-G., Wellbrock, N., 2019. Soil acidification in German forest soils. In: Wellbrock, N., Bolte, A. (Eds.), Status and Dynamics of Forests in Germany : Results of the National Forest Monitoring. Springer International Publishing, Cham, pp. 93–121.
Mols, B., Lambers, E., Cromsigt, J.P.G.M., Kuijper, D.P.J., Smit, C., 2021. Recreation and hunting differentially affect deer behaviour and sapling performance. Oikos 2022 (1).
Moomaw, W.R., 2002. Energy, industry and nitrogen: strategies for decreasing reactive nitrogen emissions. AMBIO A J. Hum. Environ. 31 (2), 184–189.
Neina, D., 2019. The role of soil pH in plant nutrition and soil Remediation. Applied and Environmental Soil Science 2019 5794869.
O'Neill, K.P., 2005. Soils as an Indicator of Forest Health: a Guide to the Collection, Analysis, and Interpretation of Soil Indicator Data in the Forest Inventory and Analysis Program. USDA Forest Service, North Central Research Station.
Plakman, V., Janssen, T., Brouwer, N., Veraverbeke, S., 2020. Mapping species at an Individual-tree scale in a temperate forest, using Sentinel-2 images, airborne Laser Scanning data, and random forest Classification. Rem. Sens. 12 (22).
Rengel, Z., 2011. Soil pH, soil health and climate change. Soil health and climate change 69–85.
Reunanen, J., 2003. Overfitting in making comparisons between variable selection methods. J. Mach. Learn. Res. 3 (Mar), 1371–1382.
Roell, Y.E., Nord-Larsen, T., Beucher, A., Greve, M.B., Greve, M.H., 2022. Mapping tree species ecograms based on soil pH and soil water availability across Denmark. Forestry: Int. J. Financ. Res. 95 (2), 287–299.
Sammut, C., Webb, G.I., 2010. Leave-one-out cross-validation. Encyclopedia Mach. Learn. 600–601.
Šestak, I., Mihaljevski Boltek, L., Mesić, M., Zgorelec, Ž., Perčin, A., 2019. Hyperspectral sensing of soil pH, total carbon and total nitrogen content based on linear and non-linear calibration methods. J. Cent. Eur. Agric. 20 (1), 504–523.
Slaton, M.R., Raymond Hunt, E., Smith, W.K., 2001. Estimating near-infrared leaf reflectance from leaf structural characteristics. Am. J. Bot. 88 (2), 278–284.
Tedersoo, L., Anslan, S., Bahram, M., Drenkhan, R., Pritsch, K., Buegger, F., Padari, A., Hagh-Doust, N., Mikryukov, V., Gohar, D., Amiri, R., Hiiesalu, I., Lutter, R., Rosenvald, R., Rähn, E., Adamson, K., Drenkhan, T., Tullus, H., Jürimaa, K., Sibul, I., Otsing, E., Põlme, S., Metslaid, M., Loit, K., Agan, A., Puusepp, R., Varik, I., Kõljalg, U., Abarenkov, K., 2020. Regional-scale in-depth analysis of soil fungal diversity Reveals strong pH and plant species effects in northern Europe. Front. Microbiol. 11, 1953.
Toro-Manríquez, M., Soler, R., Lencinas, M.V., Á. Promis, 2019. Canopy composition and site are indicative of mineral soil conditions in Patagonian mixed Nothofagus forests. Ann. For. Sci. 76 (4).
Truog, E., 1947. Soil reaction influence on availability of plant nutrients. Soil Sci. Soc. Am. J. 11 (C), 305–308.
van Straalen, N.M., Kraak, M.H.S., Denneman, C.A.J., 1988. Soil microarthropods as indicators of soil acidification and forest decline in the Veluwe area, The Netherlands. Pedobiologia 32 (1–2), 47–56.
Vrba, J., Kopacek, J., Fott, J., Nedbalova, L., 2014. Forest die-back modified plankton recovery from acidic stress. Ambio 43 (2), 207–217.
Wang, N., Xue, J., Peng, J., Biswas, A., He, Y., Shi, Z., 2020. Integrating remote sensing and landscape characteristics to estimate soil salinity using machine learning methods: a case study from Southern Xinjiang, China. Rem. Sens. 12 (24), 4118.
Webb, H., Barnes, N., Powell, S., Jones, C., 2021. Does drone remote sensing accurately estimate soil pH in a spring wheat field in southwest Montana? Precis. Agric. 22 (6), 1803–1815.
Weng, X., Li, H., Ren, C., Zhou, Y., Zhu, W., Zhang, S., Liu, L., 2022. Calcium Regulates growth and nutrient absorption in Poplar Seedlings. In: Frontiers in Plant Science, vol. 13.
Wold, S., Johansson, E., Cocchi, M., 1993. PLS: partial least squares projections to latent structures. 3D QSAR in Drug Design: Theory, Methods and Applications 523–550. . Kluwer ESCOM Science Publisher.
Zechl, W., Schneider, B.U., Röhle, H., 1990. Element composition of leaves and wood of beech (Fagus sylvatica L.) on SO2-polluted sites of the NE-Bavarian Mountain. Water Air Soil Pollut. 54 (1), 97–106.
Zhang, Y., Sui, B., Shen, H., Wang, Z., 2018. Estimating temporal changes in soil pH in the black soil region of Northeast China using remote sensing. Comput. Electron. Agric. 154, 204–212.